NEUROSCIENCE

A cerebellar adaptation to uncertain inputs

Andrei Khilkevich,[1] Jose Canton-Josh,[1] Evan DeLord,[1] Michael D. Mauk[1,2]*

Noise and variability are inherent and unavoidable features of neural processing. Despite this physiological challenge, brain systems function well, suggesting the existence of adaptations that cope with noise. We report a novel adaptation that the cerebellum implements to maintain correct responses in the face of ambiguous inputs. We found that under these conditions, the cerebellum used a probabilistic binary choice: Although the probability of behavioral response gradually increased or decreased depending on the degree of similarity between current and trained inputs, the size of response remained constant. That way the cerebellum kept responses adaptive to trained input corrupted by noise while minimizing false responses to novel stimuli. Recordings and analysis of Purkinje cells activity showed that the binary choice is made in the cerebellar cortex. Results from large-scale simulation suggest that internal feedback from cerebellar nucleus back to cerebellar cortex plays a critical role in implementation of binary choice.

INTRODUCTION

Neural activity is inherently noisy. Brain systems function well despite this, suggesting the existence of adaptations to cope with variable, uncertain inputs. Adaptations have been identified in sensory systems that help to reduce the ambiguity of signals and corruption by noise (*1*–*3*). Motor systems face an additional challenge—they must process ambiguous, noisy inputs and produce a correct motor output. This problem is related to stimulus generalization (*4*–*6*), where a neural system trained to a target input will produce lesser responses to inputs that are similar to the target. Yet, for a motor system such as the cerebellum (*7*, *8*), translating uncertain inputs into smaller amplitude outputs will result in maladaptive responses and a degradation of function. We report here a cerebellar adaptation to uncertain inputs that combines stimulus generalization with a mechanism that ensures proper output amplitude even for ambiguous, noisy inputs.

Numerous studies have demonstrated that the cerebellum learns to produce an adaptive motor output via associative learning processes (*9*, *10*). In response to a particular pattern of inputs, conveyed by mossy fibers, the cerebellum learns to produce an output of the correct amplitude (*11*). Natural input signals can be replaced by a direct electrical stimulation of mossy fibers (*12*, *13*), which has the advantage of limiting the signal to the cerebellum and providing control over the nature of the inputs. We used this advantage to study cerebellar processing of uncertain inputs using a cerebellar-dependent paradigm—eyelid conditioning. We first trained subjects to robustly respond with target response amplitude to the trained input. After that, we presented subjects with occasional probe inputs, which were systematically altered in three different ways and by a different amount from the trained input, mimicking the influence of noise and variability. We find that under these conditions, the cerebellar responses were probabilistic and bimodal, a phenomenon to which we refer as "binary choice." [The word "binary" is used here more in an illustrative way than in exact sense. There is a natural spread of conditioned response (CR) amplitudes to trained conditioned stimulus (CS) even in well-trained animals. Therefore, by binary, we mean that the distribution of CR amplitudes should be the same in response to trained CS and probe stimuli, rather than every CR is expected to be exactly target-sized.] As probe inputs become increasingly different from the trained input, the likelihood of a cerebellar response decreased, but the amplitude of responses that were produced remained at the previously trained value, maintaining the responses adaptive. We show with in vivo recordings from Purkinje cells (PCs) (the sole output neurons of the cerebellar cortex) that the binary choice computation is made in the cerebellar cortex. We used large-scale simulations of the cerebellum to explore possible mechanisms of this adaptation. Results show that these simulations display binary choice behavior only when internal feedback from the cerebellar nucleus back to cerebellar cortex is present. Combined, these results show how the cerebellum may make use of feedback to implement an amplitude completion mechanism that ensures correct output amplitudes in the face of uncertain and noisy inputs.

RESULTS

Eyelid conditioning protocols used to analyze cerebellar binary choice

Because these studies require strong control over inputs to the cerebellum, we used eyelid conditioning as a cerebellum-dependent behavior where such control is possible (*12*, *13*). In the present experiments, inputs to the cerebellum were activated via electrical stimulation of mossy fibers. The stimulation was delivered through electrodes implanted in the middle cerebellar peduncle, comprised solely of mossy fiber axons projecting to the cerebellum. The training input (CS) was a 500-ms-long 100-Hz pulse train. When repeatedly paired with a reinforcing unconditioned stimulus (US) (electrical stimulation of the skin near the eye), the training input comes to elicit predictive eyelid CRs that are mediated by the cerebellum (Fig. 1, A and B) (*14*). The training continued until CRs were near the target amplitude on almost every trial (fig. S1A).

Each subject (New Zealand albino rabbit) then received numerous sessions in which a subset of the trials involved unreinforced probe inputs that were, to varying degrees, different from the trained input. Our experiments were designed to examine cerebellar responses to systematically altered versions of the trained input. Trials with the training input were reinforced with the US to maintain high levels of responding, but all probe trials were CS-alone trials and, thus, never reinforced with US. We used three probe protocols to alter the trained input in different ways: frequency probes, short probes, and competing stimulus probes (Fig. 1, E to G), where we systemically varied probe stimulus temporal structure, duration, or overlap with the

[1]Center for Learning and Memory, The University of Texas at Austin, Austin, TX 78712, USA. [2]Department of Neuroscience, The University of Texas at Austin, Austin, TX 78712, USA.
*Corresponding author. Email: mauk@utexas.edu

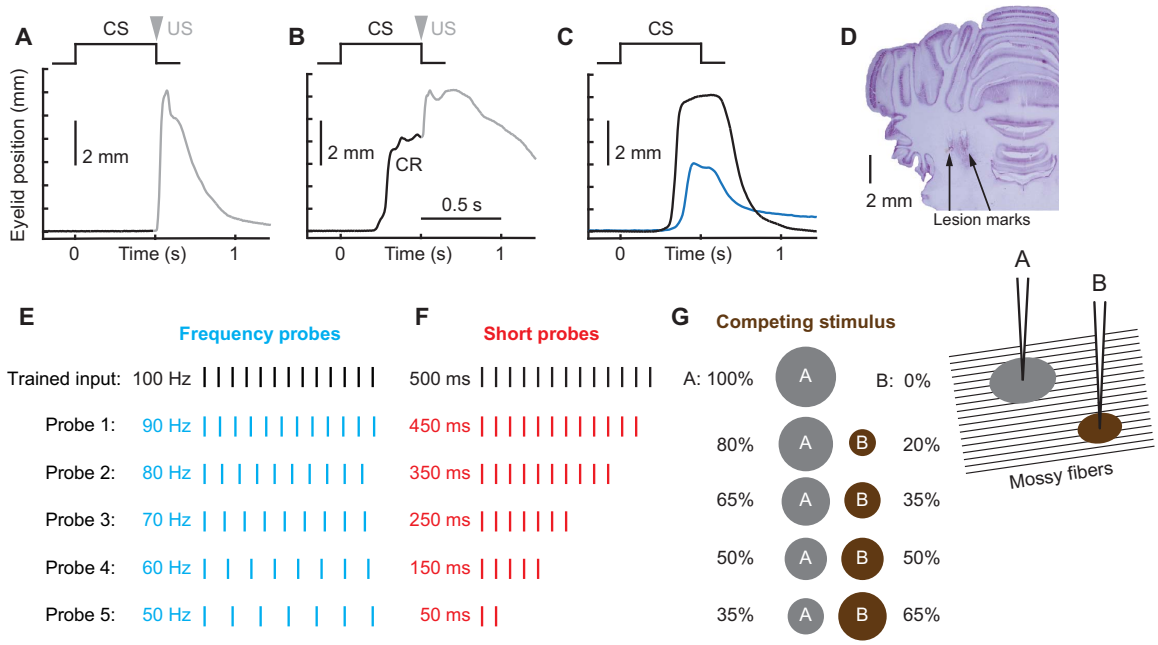

Fig. 1. Design of probe stimuli protocols. Schematics of eyelid conditioning training (**A** to **C**) and probe protocols (**D** to **G**). For (A) to (C), schematics of stimuli presentation is shown at the top, and eyelid position as a function of time is shown below. Upward deviation corresponds to eyelid closure. (A) Neutral trained input (CS) is paired with eyelid stimulation as US. In the naïve state, there is no eyelid response during CS, and the US evokes a reflexive noncerebellar eyelid closure (shown in gray). (B) Behavioral response after animal learned CS-US pairing. Predictive eyelid closure during CS and before US is a CR. (C) Example eyelid CR profiles on the CS-alone trial from subject trained to produce either a full-sized (black line) or half-sized eyelid closure (blue line). (D) Coronal histology demonstrating lesion marks from two stimulation electrodes implanted in middle cerebellar peduncle. (E to G) Schematics of probe inputs on three different probe protocols. In each case, input used for training (500-ms, 100-Hz pulse train) is shown in black. (E) Frequency probes. The length of stimulus was kept at 500 ms, but frequency was systematically decreased. (F) Short probes. Frequency was kept at 100 Hz, but only portion of the stimulus length was presented. (G) Competing stimulus. Two separate stimulating electrodes were implanted into middle cerebellar peduncle spaced 1 mm laterally. Only electrode A was used for training. During probe trials, neither frequency nor length of the stimulus was changed, but rather the current applied on electrode A was decreased and, correspondingly, the current on electrode B was increased from zero to keep the number of total activated mossy fibers approximately constant. This manipulation should result in a gradual shift of the overlap between mossy fibers activated by probe and trained stimulus. The area of current spread is illustrated as a gray circle for electrode A (used to deliver trained input) and a brown circle for electrode B (competing stimulus).

trained input, respectively. Two previous studies explored the effects of short probes (*15*, *16*), but either did not report CR amplitudes (*15*) or did not measure behavioral responses (*16*).

Under natural conditions, noise and variability along with the presence of extraneous background inputs lead to uncertainty about the representation of the training stimulus in the activity of mossy fibers. We used the probe protocols to test cerebellar responses to partially similar versions of the trained input. This could be implemented, for example, by injecting random noise into the trained input. The influence of noise, however, could be different across various time points of the trained input (a concern that is supported by the results from short probe experiments). Thus, the number of probe types required to systematically cover different noise levels across different time points precludes this approach from being feasible to implement. Instead, we opted for the control provided by systematically varying a single parameter of the trained input by a specific amount to mimic the influence of noise and variability on cerebellar inputs.

A new input that is only partially similar to the trained input creates an ambiguous situation. On the one hand, partial similarity could arise from the original learned input being contaminated by noise and irrelevant background inputs. On the other hand, there is a chance that it is a new, novel input to which the cerebellum has not yet learned a response. Furthermore, an input partially similar to the trained input should result in activation of only a subset of granule cells that are normally activated by the trained input. From the classical view of the cerebellum as a liner associative network, such partial activation of granule cells should result in decreased cerebellar output, leading to the decrease in CR amplitude and probability.

Responses to probe stimuli reveal probabilistic binary choice

However, the essential finding seen with all three probe protocols is that, although the likelihood of a CR decreased as the probes were made more different than the trained input, the amplitude of the CRs remained at the previously trained level. This is evident in the example behavioral responses from a single subject, elicited by either the trained input or 70-Hz (frequency) probes shown in Fig. 2A. The trained input elicited an eyelid CR in 92% of the trials, and the distribution of CR amplitudes (in black) showed a clear peak at 6 mm, the full eyelid closure targeted by the previous training. In turn, 70-Hz probes elicited CRs in fewer trials (46%), and the distribution of CR amplitudes (in cyan) was bimodal—with one mode being nonresponses and the second full-sized target responses. Group data for all subjects and three probe protocols are shown in Fig. 2 (B and C). For all three probe protocols, the probability of CRs decreased monotonically as the difference between the probe input and training input increased (linear fit $R^2 > 0.72$ for all probe types; Fig. 2B). The graded

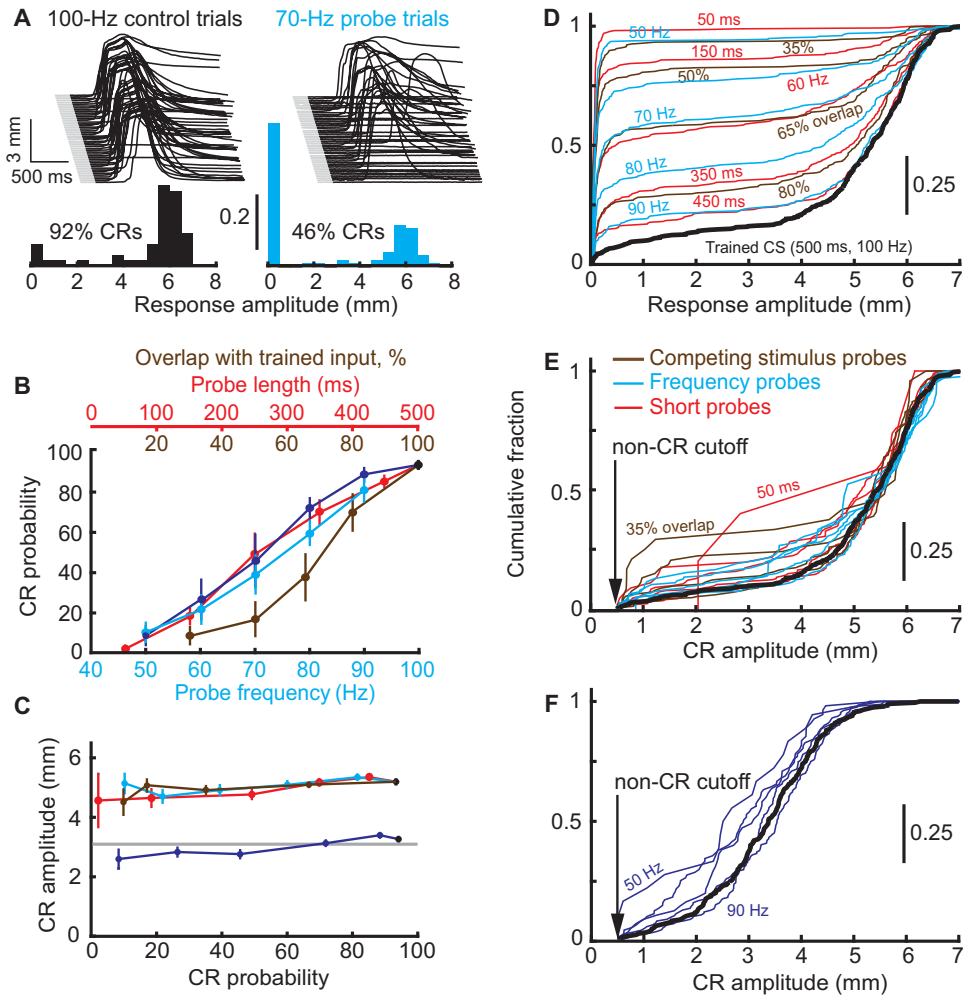

Fig. 2. Behavioral summary of binary choice. (**A**) Example eyelid responses (eyelid position as a function of time) and frequency distribution of response amplitudes to trained input (100 Hz, black, left) and to 70-Hz frequency probes (cyan, right). In about half of trials, 70-Hz probes resulted in non-CR, but CR amplitudes were all or none when they happened. (**B**) CR probability decreases as probe stimuli become more different from the trained input. Data are shown for all three protocols as follows: competing stimulus probes (brown), short probes (red), and frequency probes (cyan for animals trained to 6-mm CRs, blue to 3-mm CRs). (**C**) Mean CR amplitude as a function of CR probability remained constant in all three probe protocols, same color code as in (B). (**D**) Cumulative distribution functions (CDFs) of distributions of response amplitudes to each probe (color-coded) or trained input (black). (**E**) Same as (D), but with non-CRs removed from each distribution. (**F**) Same as (E) for rabbits trained to 3-mm target CR amplitude.

change in CR probability was not the result of averaging across subjects (fig. S2). By contrast, CR amplitudes were all or none in all three protocols, with no significant differences across different probe types and their correspondingly different CR probabilities (linear fit R^2 < 0.02 for all protocols; Fig. 2C). Even for probes that rarely elicited CRs, the amplitudes of those rare CRs were indistinguishable from those elicited by the original training input.

These all-or-none amplitudes could occur for the trivial reason that eyelid CRs are inherently all or none. Although previous studies suggest that this is not the case (*11*), we tested this directly by training a group of subjects to produce 3-mm CRs, corresponding to a half of full eyelid CR (Fig. 1C). When these subjects were tested with frequency probes (blue lines in Fig. 2, B and C), CR probability again decreased as the probes became more different from the trained input (linear fit R^2 = 0.78). CR amplitudes however remained relatively constant, independent of probe and corresponding CR probability (R^2 = 0.03). This result demonstrates that binary choice selects between a nonresponse and a response of the previously trained amplitude and is not simply a consequence of an inherently all-or-none response system. This way binary choice avoids nonadaptive expression of CRs at amplitudes different from what the cerebellum had acquired in previous training.

There is a degree of natural variability in CR amplitudes, even for the responses to the training stimulus. If binary choice operates to elicit CRs at the previously trained amplitude, then the distributions of CR amplitudes to either probe inputs or trained input should be statistically indistinguishable after non-CRs are omitted. Distributions of CR amplitudes from all protocols are shown in fig. S1. Cumulative distribution functions (CDFs) of all eyelid response amplitudes (CRs and non-CRs) for every probe protocol and type are shown in Fig. 2D. In that case, the differences between responses to trained input (black line) and probe inputs were highly significant, except for probes with parameters closest to the trained input (two-sample Kolmogorov-Smirnov test; see table S1 for *P* values). After omitting non-CR trials from distributions, all CDFs collapsed onto

the trained CS CDF (black line), as shown in Fig. 2E, and were not statistically different from it ($P > 0.1$ for 12 probes and $P > 0.05$ for 2 probes, without a correction for multiple comparisons). Similar results were obtained from the same analysis applied to the subject trained to produce 3-mm CRs (Fig. 2F and fig. S3).

Eyelid PC responses also demonstrate binary choice

The use of electrical stimulation of mossy fibers as the training and probe inputs excludes contributions to binary choice from areas upstream of the cerebellum—for example, strong mossy fiber input on CR trials and weak input on non-CR trials. To investigate possible cerebellar contributions, during binary choice probe sessions, we recorded the activity of PCs—the principle neurons and sole output of the cerebellar cortex. Tetrode microdrives were chronically implanted in six subjects, each targeting the region of cerebellar cortex previously shown (*17*, *18*) to be necessary for the expression of eyelid CRs (Fig. 3A). To ensure that analysis was limited to PCs that receive learning-related signals, we restricted analysis to "eyelid" PCs (*19*, *20*), identified by the presence of complex spikes evoked by the reinforcing stimulus (Fig. 3B and fig. S4B). Recordings from eyelid PCs during conventional eyelid conditioning sessions revealed that their activity demonstrates well-timed decreases in firing in several preparations (*16*, *19*, *21*). Moreover, the timing and magnitude of decreases in eyelid PC firing corresponded to the timing and amplitude of eyelid CRs (*19*, *21*). The ability of PCs to directly control CR kinematics and amplitude has been further demonstrated by optogenetic manipulation, where graded levels of PC inhibition produced graded response amplitudes (*22*). In other cerebellar-dependent tasks, such as smooth pursuit or saccade adaptation task, PC population activity is also directly related to the kinematics of the movement and captures high portion of behavioral variability (*23*, *24*). Finally, evidence that PCs control behavioral response amplitude comes from a series of studies (*25*–*27*), where the presence or absence of a climbing fiber input on a given trial was shown to cause an incremental change of the PC response on the next trial and an associated change in the behavioral response amplitude. Given this abundant evidence that PC responses control the timing and amplitude of eyelid CRs, we used recordings from eyelid PCs to test the hypothesis that the cerebellar cortex output will display binary choice.

During recording sessions, we implemented frequency and short probe protocols with mossy fiber stimulation inputs ($n = 4$ and $n = 4$ subjects), as well as short probes in subjects trained with a 1-kHz tone ($n = 3$). The latter experiment was included to test whether binary choice is also observed with the natural stimuli that are normally used in eyelid conditioning studies. Figure 3C shows an example raster plot from an eyelid PC along with the behavioral responses on the left. Green dots indicate the onset times of the CRs on each trial.

Sorting the trials based on CR onset times, shown in Fig. 3C (bottom), illustrates the strong, trial-by-trial relationship between eyelid PC activity and the behavior. On non-CR trials (bottom of the raster plot), eyelid PC activity barely deviated from baseline. On trials with CRs present, the onset of the decrease in eyelid PC firing rate tightly matched CR onset time. Additional examples of eyelid PC responses to different probe types are shown on fig. S5 (A to C). Average eyelid PC firing rate profiles on CR trials (cyan for frequency probes, and red and violet for short probes with mossy fiber stimulation or 1-kHz tone as a CS, respectively) and non-CR trials (black) are shown in Fig. 3 (D and E) and fig. S5 (D and E). Here, responses of all recorded

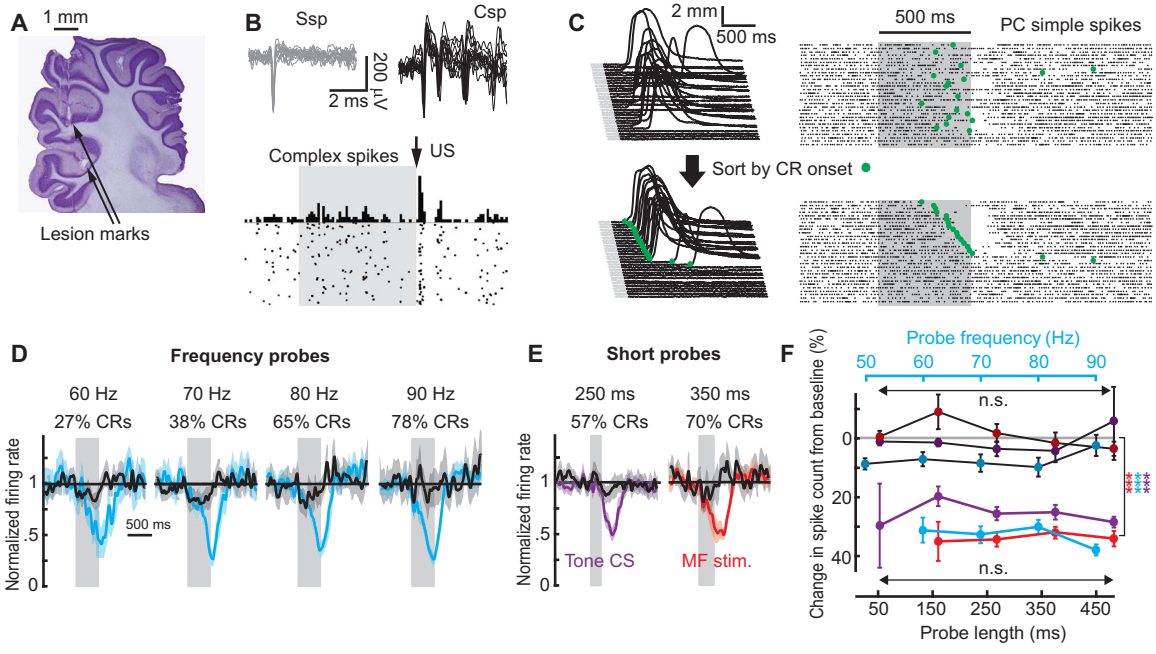

Fig. 3. In vivo recordings from PCs during binary choice sessions. (**A**) Sagittal view of histology with tetrode tracks in the cerebellar cortex. (**B**) Twenty overlaid waveforms of simple (gray, Ssp) and complex (black, Csp) spikes are shown on top, and peristimulus time histogram (PSTH) of US-evoked complex spikes from eyelid PC is shown below. (**C**) Behavior and raster plot of PC simple spikes during CS-alone frequency probe trials. Trials are sorted either in order of occurrence (top) or according to CR onset time (green dots, bottom). (**D**) Average firing rate of eyelid PCs on CR (cyan) or non-CR trials (black) during frequency probes. Gray region represents probe duration. Shaded regions indicate 95% confidence intervals. (**E**) Same as (D), but individual examples for short probes, using either mossy fiber (MF) stimulation (red) or 1-kHz tone (violet). (**F**) Average spike count of eyelid PC activity on CR (color-coded by probe protocol) and non-CR trials (black lines, darker-colored points to indicate the protocol).

eyelid PCs were combined across trials with the same probe type. In all cases, the responses of eyelid PCs showed clear differences on CR versus non-CR trials. To quantify this effect, we calculated average spike counts on CR and non-CR trials over a 700-ms window from CS onset, shown in Fig. 3F. For all protocols, there was highly significant difference between spike counts on CR versus non-CR trials [two-way analysis of variance (ANOVA), $P < 10^{-13}$ in each case; see table S2]. The decreases in PC activity on CR trials were indistinguishable across the different probes and CR probabilities (two-way ANOVA, $P > 0.2$ for all protocols), directly paralleling behavioral binary choice. Previous work (*19*, *21*) demonstrated that eyelid PC responses vary with CR amplitude. The present data demonstrate that this relationship does not break down during binary choice. Combined with the use of mossy fiber stimulation as the trained and probe inputs, these data are consistent with binary choice as a cerebellar-mediated phenomenon.

As a further test that the cerebellar cortex computes binary choice, we tested whether CR versus non-CR trials can be predicted from PC activity on a trial-by-trial basis. If binary choice is computed by the cerebellar cortex, then these predictions should be equally strong across different probes that give rise to different CR probabilities. To test this hypothesis, we used receiver operating characteristic (ROC) analysis (*28*, *29*), a tool commonly used in decision-making studies. Spike count distributions from eyelid PCs on CR (cyan and violet) and non-CR (black) trials are shown in Fig. 4A for two probe types. We calculated spike counts over 700 ms from CS onset. On the basis of such distributions, we constructed ROC curves and calculated choice probabilities as an area under the ROC curve (AUC). Figure 4B shows a summary over every probe type that produced sufficient number of CRs on recording sessions. Choice probabilities for every probe type were significantly above chance (permutation test, 5000 samples), with $P < 0.001$ for three "middle" probes with CR probability near 50% for all three protocols. The ability to predict a behavioral response was not different for all probes within each protocol ($P > 0.4$ for all pairwise comparisons in each protocol; permutation test, 5000 samples), consistent with the hypothesis that cerebellar cortex implements binary choice.

Changes in eyelid PC activity precede behavioral responses

The phenomenon of binary choice can be broken down in two components: the CR no-CR decision itself and the binary expression of response amplitude. Results above showed that cerebellar cortex output displays the binary response amplitudes. To address the decision component of the phenomenon, we investigated the time course of behavioral decision readout from PCs. For that, we calculated choice probability value as a function of time. PC activity on each probe trial was aligned either by the onset of the mossy fiber stimulation or by CR onset for that trial, then spike trains were divided into a series of 100-ms nonoverlapping time windows, and choice probabilities were calculated over each time window. For data aligned by the onset of probe input (Fig. 4C), the probability of correctly predicting CRs versus non-CRs rose above chance after 200 ms from input onset and peaked near input offset. When aligned to CR onset (Fig. 4D), for all three protocols, choice probabilities showed above chance values at least 100 ms before CR onset ($P < 0.001$, permutation test, 5000 samples). This result suggests that the initiation of behavioral decision is also done by cerebellar cortex. The prediction accuracy peaked (AUC = 0.87 ± 0.04) at 200 ms after CR onset, corresponding to the time of peak eyelid velocity.

In summary, combining the use of electrical stimulation of mossy fibers as trained and probe inputs, which bypassed sensory processing, with recordings from PCs demonstrates that binary choice is a computation that involves the cerebellar cortex. These results do not imply, however, that PC responses are bistable (*30*) or that cerebellar output itself has an inherently binary nature. Instead, our results demonstrate a cerebellar ability to elicit a response at the previously trained amplitude even for mossy fiber inputs that have a relatively low probability to elicit that response. The adaptive advantage of this computation is to prevent the expression of responses with nonadaptive amplitudes when noise creates uncertainty about the nature of input.

Results of cerebellar simulation suggest that deep cerebellar nucleus feedback is necessary for binary choice

One advantage of using eyelid conditioning to study the cerebellum is the availability of large-scale simulations (*31*, *32*) of the cerebellum, developed over 20 years, that have been shown to capture many behavioral aspects of eyelid conditioning (*9*, *13*, *31*). We used large-scale cerebellar simulation to test a mechanistic hypothesis of how the cerebellum implements binary choice computations. The simulation is composed of over 10^6 (over 2^{20}) spiking, conductance-based neurons and implements known connectivity rules of the cerebellum within the limits of the simulation size (see Materials and Methods). From the simulation, we can monitor spiking activity of any (or all)

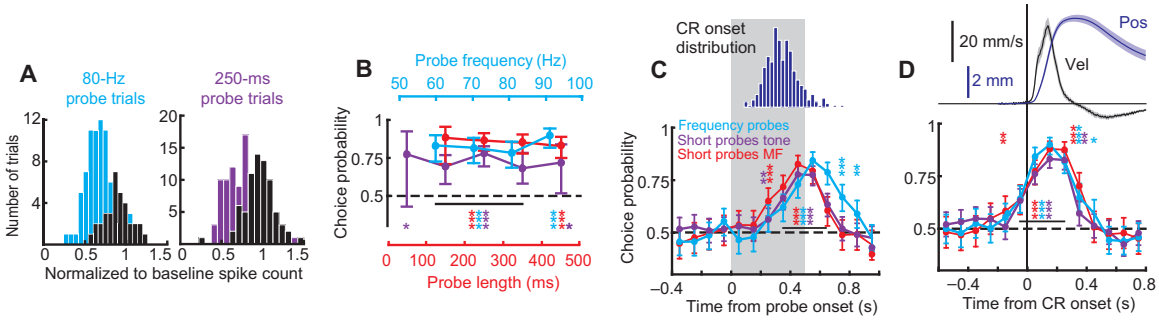

Fig. 4. ROC analysis of PC activity. (**A**) Frequency distributions of PC spike counts on CR (color) and non-CR trials (black). (**B**) Choice probability calculated using ROC analysis for each probe type within three probe protocols. (**C**) Choice probability as a function of time, using 100-ms time bins. Here, for each protocol, we combined trials from three middle probes; identical results were also obtained in analyses of individual probes (fig. S6). Spike trains are aligned to probe onset. Points are plotted in the center of their corresponding bin. Distribution of CR onset times is shown on top. (**D**) ROC analysis of the same data but with trials aligned by behavioral CR onset (black vertical line). Error bars indicate 95% confidence intervals. Significance above chance at 0.05, 0.01, and 0.001 is depicted by one, two, or three asterisks, respectively.

neuron(s) along with virtual eyelid position calculated from simulation deep cerebellar nucleus (DCN) output.

A feedback mechanism can implement all-or-none decision at a circuit level (*33*). We hypothesized that the recently characterized axon collaterals (*34*, *35*) of DCN neurons (DCNcol) (fig. S7A) could act in a similar manner during binary choice. The DCNcol axons synapse on granule and Golgi cells in cerebellar cortex with normal mossy fiber properties. In this way, mossy fiber inputs driven by CR expression provide a positive feedback to the cerebellar cortex that could serve as additional input to guide learning.

We constructed two types of simulations that differed only by the presence or absence of DCNcol (fig. S7A). Both simulations acquired full-sized CRs at a similar rate when given the same training used in our experiments (fig. S7, B and C). After acquisition, we presented probe stimuli using the same three binary choice protocols used in the experiments. For all three protocols, the simulation with DCNcol (Fig. 5A) displayed robust binary choice: Although CR probability varied with the probes, CR amplitude remained at a relatively constant value. In contrast, binary choice responding broke down in simulations lacking DCNcol—as probe inputs became more different than the training input, CR amplitudes systematically decreased (Fig. 5B).

To quantify the degree of independence of CR amplitudes (or PC responses) from CR probability, and to compare data across experiments and simulations, we developed a binary index measure (BI, see Materials and Methods). By design, BI = 1 corresponds to full independence, where CR amplitudes do not change as CR probabilities change. Conversely, BI = 0 corresponds to CR amplitude decreasing at the same rate as CR probability, and BI < 0 corresponds to a more abrupt decrease in CR amplitude than probability (fig. S8, A and B). Both experimental data and data from simulations with DCNcol showed BI close to 1, while simulations lacking DCNcol had near-zero or negative BI (Fig. 5C). We applied the same analysis to PC responses from simulations and from real recordings. Similar to the behavioral data, the responses of real PCs and virtual PCs from simulations with DCNcol were largely the same on CR trials, independent of probe and CR probability (Fig. 5, D and F). By contrast, in simulations without DCNcol, PC responses gradually changed with CR probability (Fig. 5, E and F). Finally, we also applied ROC analysis to PC responses from the simulation with DCNcol and obtained results indistinguishable from analysis of real PC recordings (fig. S9).

DISCUSSION

In these studies, we used advantages of eyelid conditioning to investigate cerebellar adaptations to noise and the input ambiguity that noise causes. Several studies have addressed this question in some way using different cerebellar-dependent paradigms: vestibular-ocular reflex learning (VOR) (*36*), smooth pursuit (*37*), or eyelid conditioning (*16*, *38*, *39*). In the studies of Guo *et al.* (*36*), Medina and Lisberger (*37*), and Garcia *et al.* (*39*), a visual or auditory stimulus was used in behavioral paradigms, which made it impossible to explicitly disassociate the cerebellar contribution from transformation done by the sensory systems upstream from the cerebellum. To overcome this limitation, we used direct electrical stimulation of mossy fibers as the trained and probe inputs to the cerebellum. To mimic the effects of noise, we systematically varied the difference between probe inputs and the trained input. Not surprisingly, we found that the likelihood of CRs decreased as the probes became less similar to the training stimulus. Although the traditional linear associative network view of the cerebellum would predict otherwise, we found repeatedly that the cerebellum implements a mechanism to maintain the proper (previously trained) amplitude of CRs even for probes that rarely elicited responses. This appears to represent a novel computational adaptation to limit the deleterious effects of noisy inputs.

We found that eyelid PCs, the sole output neurons of cerebellar cortex, also displayed the binary choice. Moreover, changes in PC activity preceded behavioral responses, suggesting a causal relationship. While the binary choice can be read out from eyelid PCs, this does not necessary imply that the computation is entirely implemented

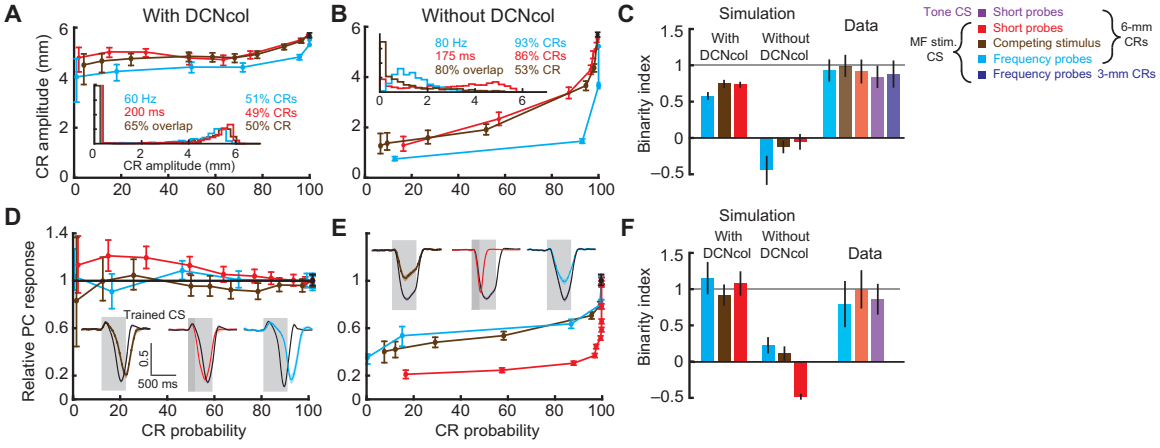

Fig. 5. Simulation with DCNcol replicates binary choice phenomenon. (**A**) Dependence of CR amplitude on CR probability in simulation with DCNcol. Results are shown for the same three probe protocols used in experiments. Color-coding is preserved as in Fig. 1 and further explained in the legend on the right. Inset: Distribution of CR amplitudes in response to one probe type per protocol, indicated above distribution. Error bars indicate 95% confidence intervals. (**B**) Results of the same experiments performed in simulation without DCNcol. (**C**) Comparison of behavioral results using binarity index (BI). Results are shown for two types of simulations and experimental data (lighter bars). Error bars show 1 SD. MF, mossy fiber. (**D**) Decrease in simulation PC activity on probe trials with CRs as a function of CR probability. Insets: Average normalized firing rate of simulation PCs on CR trials, in response to trained CS (black) and probes (colored). (**E**) Same as (D), but for simulation without DCNcol. (**F**) Same metric and layout as in (C), but here eyelid PC activity was used to determine the degree of binarity of PC responses.

within the cerebellar cortex. A hypothesis, supported by the results from cerebellar simulations, suggests that while the initiation or absence of CR is determined within the cerebellar cortex, the later portion of CR determining the final amplitude relies on feedback from cerebellar nuclei neurons.

The simulation results suggest that DCNcol do not act as a gain modulator, as suggested previously (*40*). Among other things, this would produce true bistability with CRs being all or none rather than previously trained target or none. Instead, a feedback input driven by DCNcol will activate a separate subset of granule cells (*41*) and can serve as an additional signal that contributes to learning the latter portion of a response (Fig. 6). In this way, the onset of a CR is driven by CS-activated mossy fiber input (Figs. 4D and 6B), while the later portion of a CR can be driven by DCNcol mossy fiber feedback (Fig. 6C). Thus, without a DCNcol contribution, inputs that differ from a previously trained input can give rise to smaller-than-trained response amplitudes. With the influence of DCNcol, noisy inputs that would have otherwise produced a range of CR amplitudes need to only initiate a response. Once a CR begins, DCNcol feedback provides a signal back to the cerebellar cortex that, through previous learning, is capable of driving the CR output to its target, previously trained amplitude. We propose therefore that one functional property of DCNcol is to implement an "amplitude completion" mechanism that contributes to the adaptive binary choice computation displayed by the cerebellum.

According to this hypothesis, the contribution of DCNcol to the behavioral response will progressively increase with additional training. While the purpose of extensive training to the trained input in our experiments was to narrow down the distribution of CR amplitudes, it could be that such extensive training is required to clearly observe the reported binary choice phenomenon. Previous work (*40*) demonstrated that optogenetic silencing of DCNcol in mice results in a reduction, but no abolishment, of CR amplitudes. We hypothesize that the effect would be even more prominent in mice trained to the asymptotic performance.

Many of the mechanisms and computational properties of cerebellum have been found in parallel across different cerebellar tasks, such as VOR adaptation, saccade adaptation, smooth pursuit learning, and eyelid conditioning. Two prominent examples are (i) the existence and rules of the plasticity sites in the cerebellar cortex and cerebellar nuclei (*42*–*44*) and (ii) the single-trial effect, where the presence or absence of climbing fiber input on a given trial was shown to cause an incremental adjustment of behavioral output (*25*–*27*, *45*) and PC response (*25*–*27*) on the next trial. There has been generally a good agreement among the data from these tasks, despite the difference in involved motor systems. This gives no reason to suspect that the reported results are in some way specific to eyelid conditioning. For example, control experiments showed that the binary choice phenomenon is not a trivial consequence of eyelid responses being inherently all or none. We would like to point out though that the experiments described here were designed to mimic learning of a single correct motor response for a specific input. In this scenario, our data demonstrated that the responses to a partially similar input are bimodal: with one mode corresponding to the same amplitude as was learned with the trained input and the second mode being nonresponses, since the cerebellum had learned to produce the responses only to the trained input. Further studies are needed to investigate how the binary choice process plays when several responses are learned or multijoint and/or multicomponent movements are involved.

The presence of an amplitude completion mechanism in the cerebellum suggests that the cerebellum and hippocampus display a parallel sequence of computational operations. In the cerebellum, the granule cell layer has long been implicated in pattern separation, a process that recodes similar mossy fiber inputs into less similar patterns of granule cell activity, presumably in the service of better discrimination (*8*, *46*). Our results reveal a form of pattern or, in this case, amplitude completion downstream from pattern separation. In the hippocampus, granule cells in dentate gyrus are thought to implement pattern separation, while the next stage of processing in the CA3 region is thought to implement pattern completion (*47*). The sequence of pattern separation followed by pattern/amplitude completion may help to discriminate between similar inputs, while ensuring that a proper "completed" response is produced if the similarity is

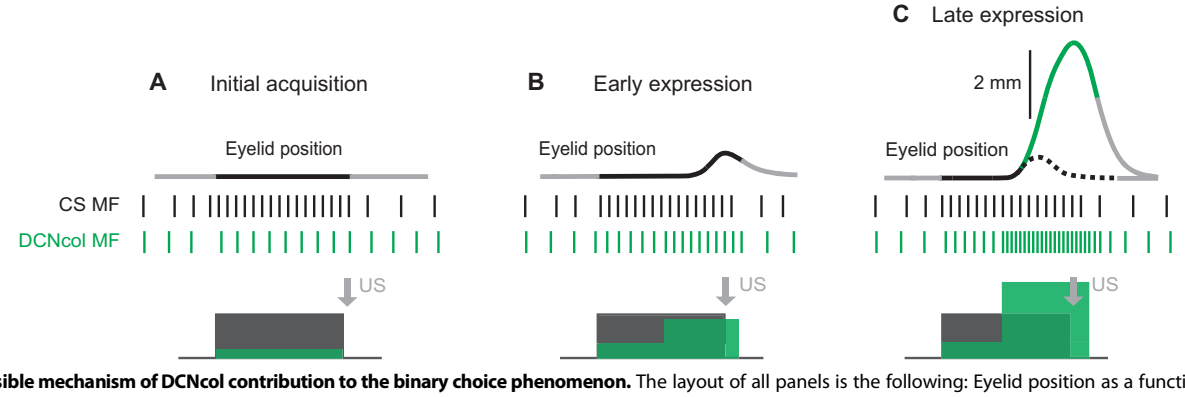

Fig. 6. Possible mechanism of DCNcol contribution to the binary choice phenomenon. The layout of all panels is the following: Eyelid position as a function of time is shown on top, with a region colored in black indicating the duration of CS. Vertical lines in the middle represent spike train inputs from CS-activated mossy fibers (MFs) (black) and DCNcol MFs (green) to the cerebellar cortex. Correspondingly, colored rectangles below show schematized PSTHs. The time of US delivery is shown by a gray arrow. (**A**) Initial acquisition. Since CRs have not developed yet, CS-activated MFs are the main input that the cerebellum is learning to. (**B**) Early expression. As small amplitude CRs start to happen, the cerebellum starts to get two kinds of inputs: (i) MF activated by CS (black) and (ii) DCNcol MFs (green). Initially, small CRs are associated only with CS, since that was the only input present during initial acquisition. (**C**) Late expression. As CR amplitude increases, so does DCN activity that drives CR and, therefore, also DCNcol input (green) to the cerebellar cortex. After acquisition is complete, only the early portion of CR is associated with CS (black portion of eyelid position profile), while the later portion of CR—which determines its amplitude (green portion)—is associated with DCNcol feedback input. Dashed black line represents a schematized CR profile that would be present if DCNcol feedback was disabled.

sufficient. These apparent parallels may reflect somewhat general mechanisms for minimizing the detrimental influence of noise on the performance of brain systems.

MATERIALS AND METHODS

Subjects

The subjects were 22 male New Zealand albino rabbits (*Oryctolagus cuniculus*; Myrtle's Rabbitry) weighing 2 to 3 kg at experiment onset. Treatment of rabbits and surgical procedures were in accordance with the National Institutes of Health guidelines and an institutionally approved animal welfare protocol. All rabbits were maintained on a 12-hour light/dark cycle.

Surgery

One week before the start of the experiment, rabbits were removed from the home cage and anesthetized with a cocktail of acepromazine (1.5 mg/kg) and ketamine (45 mg/kg). After onset of anesthesia, the rabbits were placed in a stereotaxic frame, intubated, and maintained on isoflurane (1 to ~2% mixed in oxygen) for the remainder of the surgery. Under sterile conditions, the skull was exposed with a midline incision (~5 cm), and four holes were drilled for anchor screws. Some anchor screws also functioned as ground screws for rabbits with mossy fiber stimulation implants or a microdrive ground for rabbits with microdrive implant. The rabbit's head was then positioned with lambda 1.5 mm ventral to bregma. For rabbits prepared only for behavioral experiments involving electrical stimulation of mossy fibers, a craniotomy was drilled out at 5.5 mm lateral and 3 mm anterior from lambda, ipsilateral to the trained eye. For rabbits prepared for microdrive implantation, a craniotomy was also drilled out at 5.9 mm posterior and 6.0 mm lateral to lambda. Skull fragments were carefully removed from the craniotomies, and the dura matter was carefully opened under visual guidance. One (2 rabbits) or two laterally spaced (1 mm, 19 rabbits) tungsten stimulating electrodes (A-M Systems; tip exposed to obtain impedance of 100 to 200 kilohm) were implanted in the middle cerebellar peduncle (16 mm ventral to lambda). A custom-made microdrive (16 tetrodes and 2 references) fitted with an electronic interface board (EIB-36-16TT, Neuralynx) was implanted in the left anterior lobe of the cerebellar cortex at a 40° angle posterior to vertical and 17.8 mm ventral to lambda. This region of the anterior lobe has been shown to be involved in acquisition and expression of well-timed conditioned eyelid responses (*13*, *18*, *19*). The primary target of the tetrode recordings were PCs with evoked complex spikes from US. The bundle cannula of the microdrive was lowered to the surface of the brain, and the craniotomies were sealed with low viscosity silicon (Kwik-Sil, World Precision Instruments). The head bolt to mount eyelid detector, anchor/ground screws, stimulation electrodes, and microdrive were secured with dental acrylic [Bosworth Fastray (Pink), The Harry J. Bosworth Company], and the skin was sutured where the skull and muscle were exposed. Finally, two stainless steel loops terminating in gold pins were inserted into the anterior and posterior periorbital region of the left eye for delivery of the stimulation US. Rabbits were given postoperative analgesics and antibiotics for 2 days after surgery and were allowed to recover for a week before experiments began.

Conditioning

The rabbits were trained in custom-designed, well-ventilated, and sound-attenuating chambers measuring 90 × 60 × 60 cm (length × width × height). Each rabbit was placed in a plastic restrainer, with their ears stretched over a foam pad and taped down to limit head movement. To measure eyelid position, we attached an infrared emitter/detector system directly to the head stage of each rabbit to record movements of the left external eyelid. These detectors provide a linear readout of eyelid position (±0.1 mm) at 1-kHz sampling rate by measuring the amount of infrared light reflected back to the detector, which increases as the eye closes (*48*). At the start of each daily session, the gain of the eyelid position detector was calibrated by delivering a test US to elicit full eyelid closure (defined as 6.0 mm, typical for an adult rabbit). A trial would not start until the rabbit's eyelid was sufficiently open. Stimulus presentation was controlled by custom-designed software for all experiments.

Experimental design

Initial training

For initial training, rabbits were given daily eyelid conditioning sessions composed of 12 blocks of nine trials each. For rabbits trained to produce full-sized CRs, each block consisted of one CS-alone trial and eight paired trials (CS + US). For rabbits trained to make half-sized (3 mm) CRs, a block consisted of one CS-alone trial and eight trials, which were either a paired or a CS-alone trial, depending on the CR amplitude before the US delivery. Following published training procedure (*11*), eyelid position was monitored throughout the presentation of the CS, allowing us to calculate the CR amplitude. If CR amplitude was equal to or larger than the target (3 mm) 10 ms before US presentation, then the US was skipped at that trial. Otherwise, if the CR size was too small, then the US was presented at the end of the CS. All rabbits were trained at an interstimulus interval (ISI) of 500 ms. Each conditioning chamber was equipped with a speaker that was connected to a stereo equalizer and receiver, which were connected to a computer that generated the tone. For rabbits trained using tone as the CS, the CS was set as a 1-kHz, 500-ms, 75-dB sinusoidal tone with a rise and fall time of 5 ms to avoid audible clicks from the speaker. For rabbits trained with mossy fiber stimulation, the trained CS was a constant frequency pulse train of cathodal current pulses (100 Hz, 500 ms, 0.1-ms pulse width, 100 to 150 μA), generated by a stimulus isolator (model 2300, A-M Systems) and passed through the electrode(s) implanted in the middle cerebellar peduncle. The current pulses were controlled by custom-written software and delivered through an isolated pulse stimulator (model 2100, A-M Systems). Electrical leads from a separate stimulator (model 2100) were attached to the periorbital electrodes to deliver pulses of electrical stimulation to the left eyelid as the US. The US was a 50-ms train of constant current pulses (50 Hz, 1-ms pulse width, 1 to 3 mA) delivered through the periorbital electrodes. US intensity was adjusted for each rabbit to produce a full eyelid closure without any pain reactions. All types of trials in all sessions were separated by a mean intertrial interval of 30 ± 10 s. The period of initial training was not fixed but rather continued for each rabbit until both CR percentage was high (CR% > 90%) and CR amplitudes were robust and near the target amplitude (fig. S1A). Typically, such initial training lasted for 10 sessions from a naïve state.

Probe sessions

After the initial training was complete, the rabbits were switched to probe sessions. Each probe session included 30 CS-alone probe trials interspersed with 80 paired trials. For rabbits trained to half-sized CRs, only a portion of the 80 trials were paired depending on the CR amplitude on a given trial as described above. The purpose of the paired

trials during the probe sessions was to maintain the high level of CRs to trained stimulus. While we would want to include as many CS-alone probe trials in the session as possible, it is important that probes were infrequent enough that they did not change responding during the session because of the extinction effect. Our studies showed that for well-trained rabbits, having 30 probe trials per session fulfills this requirement.

We implemented three probe protocols that systematically altered the probe stimulus from the trained CS in different ways: (i) Probe durations ranged from 50 to 450 ms in 50-ms increments (short probes); (ii) probe duration was not changed from the trained CS, but stimulation frequency was decreased from the original 100 Hz down to 50 Hz in 10-Hz increments (frequency probes); and (iii) the temporal pattern of the trained CS (duration and frequency) was unaltered (competing stimulus probes). However, the current intensity delivered through stimulation electrodes was adjusted to gradually shift the population of activated mossy fibers, maintaining only a partial overlap with mossy fibers used for training (Fig. 1G). Specifically, the current intensity delivered through the electrode used in training was decreased on probe trials, but an additional "competing" input through the second electrode, which was not used during acquisition, was delivered to maintain approximately the same total amount of activated mossy fibers by trained CS and the competing stimulus probes. We used here a simple assumption that the number of activated mossy fibers is determined by the area of current spread, the diameter of which is proportional to the current intensity

$$N \sim d^2 \sim I^2$$

where N is the number of activated mossy fibers, and I is the current intensity applied through the electrode. Such an assumption was our best approximation to maintain the same number of activated mossy fibers across all probe types. Only one type of probe protocol was used in a single probe session. However, the same rabbits were often used in sessions with different probe protocols. Typically, five probe types (for example, 50, 60, …, 90 Hz) were presented during the session, with six probe trials per probe type per session. Such sessions were repeated several times for each rabbit to collect a sufficient amount of probe data. Some probe sessions also included CS-alone trials with trained CS. Responses to the trained CS were extracted from these sessions and from CS-alone trials during normal training sessions that directly preceded, followed, or were in-between the sequence of probe sessions.

In vivo recordings and unit isolation

The details about recordings procedure, single-unit isolation, and identification of eyelid PCs have been published previously (*19*). Briefly, each independently movable tetrode in a microdrive was composed of four nichrome wires (12-μm diameter; Kanthal Palm Coast). These were twisted and then heated so that the insulation was partially melted together to form a tetrode. The individual wires of each tetrode were connected to the EIB with gold pins. Each tetrode was gold-plated to reduce final impedance to 0.5 to 1 megohm measured at 1 kHz (nanoZ kit, Neuralynx). During surgery, the tetrodes were placed over the target site of the left anterior lobe of the cerebellar cortex and were advanced to within 2.0 mm ventrally from the target during surgery using stereotaxic guidance. After recovery from surgery, each tetrode was lowered in 40- to 80-μm increments per day until at least one stable single unit was identified, although there were often multiple units on a single tetrode. The tetrodes were allowed to stabilize for 24 hours, and units were checked again before recording and behavioral training commenced. A custom-written cluster cutting program was used to isolate single units offline. Commonly used waveform features, such as peak, valley, and energy, were used during cluster cutting. Additional features, such as the late peak measure (*19*), were used to identify complex spikes and differentiate them from simple spikes. In some cases, complex spikes formed a separate cluster from simple spikes when viewed in the peak, valley, or energy planes. Belonging of putative simple and complex spikes to the same PC was verified by computing a spike-triggered average of simple spikes on complex spikes, demonstrating a post-complex spike pause (fig. S4B) (*20*). Eyelid PCs were defined by the presence of US-elicited complex spikes as shown in Fig. 3B. The remaining PCs were considered "non-eyelid." We recorded 491 single units during the binary choice sessions. Of those, 82 units were classified as eyelid PCs and 116 units as non-eyelid PCs. All single-unit analyses reported in the paper were performed on simple spikes from eyelid PCs. Recordings where the unit was lost at any time during the session were not included in the analysis.

Data analysis

Following cluster cutting, all subsequent data analysis was performed using custom-written scripts in MATLAB.

Eyelid data analysis

For each trial, 2500 ms of eyelid position data (200 ms pre-CS, 2300 ms post-CS) were collected at 1-kHz sampling rate and at 12-bit resolution. The data were stored to a computer disk for subsequent offline analysis. Eyelid position data were passed through a low-pass Savitzky-Golay filter. A small fraction of trials that had eyelid movement during the 200 ms before the CS onset were discarded. For every trial, we calculated CR amplitude and CR onset time. Because we used only CS-alone trials in all steps of analysis, CR amplitude was defined as the maximum value of eyelid position from the baseline, calculated between CS onset and 500 ms after CS offset. An eyelid response was counted as a CR if the CR amplitude reached the 0.5-mm criterion. The CR onset time was defined only for CR trials and was determined using a custom-written two-step algorithm. The first step was designed to detect the initial deflection of eyelid position away from the pre-CS baseline, while the second step used linear interpolation to determine the exact time of CR onset.

Binary index measure

For every probe protocol, we calculated a dependence of CR amplitude on CR probability, where each probe type contributed a single point on the plot (Figs. 1C and 5, A and B). In the ideal implementation of binary choice, CR amplitude would be constant over the whole range of CR probabilities, that is, CR amplitude would be independent from CR probability (fig. S8B, black squares). To quantify the degree of dependence of CR amplitude on CR probability, we calculated the BI. BI was defined as the area between CR amplitude curve (fig. S8A, right, red line) and the diagonal line (gray), connecting a point corresponding to the trained CS with the point of origin. Red-shaded area in fig. S8A illustrates the description. The measure was normalized so that the ideal BI (black-shaded area) is equal to one. To evaluate the expected mean and SD of BI, we drew 1000 samples of 50 random trials per each probe type within a protocol, and, for each sample, BI was calculated as described above. For each sample, if the fraction of CRs was less than 10% for a particular probe, then it was not included in the BI calculation.

The BI measure was also used to evaluate the independence of PC responses from CR probability. The BI definition there was identical, except CR amplitude was replaced with "relative PC response" (Fig. 5,

D and E). Relative PC response was defined (fig. S8C) as the ratio between (i) mean decrease from baseline in PC spike count on CR trials in response to trained CS (black dots in scatter plot) and (ii) decrease in spike count on CR trials in response to probe stimuli (red dots in scatter plot).

Single-unit data analysis

Spike times of individual PCs were synchronized with recordings of eyelid position and stimuli onset/offset times. Instantaneous firing rate of each PC was estimated on every trial using an inverse of the interspike interval, followed by a two-sided Gaussian kernel with a 20-ms SD window. For every PC, the firing rate was normalized by the value of the baseline firing rate during 1500 ms of pre-CS activity.

ROC analysis

Because the data that we observed resembled probabilistic decision-making, we used analyses from signal detection theory, which are commonly used in decision-making studies. To quantify the relationship between eyelid PC activity and behavioral responses, we used an ROC analysis. For each probe stimulus type, the trials were grouped into two groups based on the behavioral responses: CR trials or non-CR trials. Note that such grouping only assures the presence of a CR on a CR trial but does not assure specific CR amplitude. Because by the session's design there were only six trials per probe type per session (and therefore per individual PC), we did not compute an ROC curve separately for each cell. Instead, we combined spike counts from all recorded eyelid PCs on different sessions into a single "grand" distribution for each probe. A session was added into the grand distribution only if at least one CR and one non-CR were present on a given probe type trials. For each recorded eyelid PC, spike counts were normalized to the average spike count during the pre-CS baseline. Such normalization allowed us to reduce the influence of the baseline firing variance in different PCs on the shape of the grand spike count distribution. ROC curves were calculated from the spike counts of the grand distributions, and an AUC was calculated to measure the probability of correct prediction of the behavioral outcome (CR versus non-CR) from PC spike count on a random trial. Note, however, that the resultant AUC from the grand distribution can only be less than the mean across AUC values computed for each cell separately. Therefore, AUC values reported here, referred to as choice probabilities, represent a lower estimate of the mean choice probability across the eyelid PC population. To measure an overall ability to predict the behavioral outcome, we calculated PC spike counts over 700 ms from the CS onset window. To quantify a finer temporal structure of choice probability, we calculated spike counts over nonoverlapping 100-ms time windows and used an ROC analysis on each window separately in the same fashion as described above. To align spike trains on non-CR trials to CR onset time, for each non-CR trial, we randomly drew 1000 times with replacement from CR onset distribution, calculated an aligned to CR onset spike train for each draw, and, finally, computed the mean aligned to CR onset spike train. Error bars shown for AUC values represent 95% confidence intervals calculated by bootstrapping 1000 samples. Permutation test was used to measure significance above chance (5000 samples).

Computer simulations

We used a large-scale simulation of the cerebellum (over 10^6 simulated neurons) to test the hypothesis about a contribution of DCNcol to the binary choice phenomenon. These simulations were composed of conductance-based, single-compartment, spiking representations of neurons. The properties of the simulation were intended to emulate the synaptic organization and physiology of the cerebellum [for example, see (*49*)]. Connectivity between neuronal types in the simulation mimicked known facts about cerebellar circuitry [for details, see the study of Li *et al.* (*32*)]. As an approximation to the ratio of cell types within the cerebellum, the simulation was composed of 1024 mossy fibers, 1,048,576 (2^{20}) granule cells, 1024 Golgi cells, 128 basket cells, 512 stellate cells, 32 PCs, 8 deep cerebellar nuclei cells, and 32 climbing fibers. These neurons were interconnected to emulate a parasagittal stripe, where all PCs receive input from climbing fibers of the same type—that is, all PCs in the simulation were eyelid PCs per the definition used for in vivo recordings.

A new addition in the current version of simulation is the presence of DCNcol that projected as mossy fibers back to the granule-Golgi cell network. We implemented 30 DCNcol in the simulation. DCNcol had the same connectivity to Golgi and granule cells as normal mossy fibers, but the spiking activity conveyed by each of them was a copy of one of the eight DCN neurons (chosen randomly at simulation initialization). In this way, we have incorporated axon collaterals only from glutamatergic DCN neurons (*34*, *40*), leaving contributions from GABA (γ-aminobutyric acid)/glycinergic neurons (*35*) aside.

The state of the network was updated every millisecond. The only external inputs to the simulation were the spiking activity of 1024 mossy fibers and 32 climbing fibers, one per each PC. Synaptic plasticity sites were implemented at the granule cell–to–PC synapses and at the mossy fiber–to–DCN synapses. A granule cell–to–PC synapse underwent long-term depression (LTD) or long-term potentiation (LTP) every time a granule cell fired a threshold burst of spikes: LTD occurred if this burst fell within a window between 200 and 100 ms before a climbing fiber input to the PC; otherwise, LTP occurred. Mossy fiber–to–DCN synapses active within a time window of an abrupt pause in PC activity underwent LTP, whereas those active during a strong increase of PC activity underwent LTD.

To train the simulation, we assigned 25 mossy fibers to be CS-driven. These mossy fibers changed their firing rate from 5 to 60 Hz for the duration of the CS. Spike times for each mossy fiber were determined from a Poisson distribution with a given mean. The only exception was the CS-driven mossy fibers in simulations trained for the frequency probes experiment. To directly replicate these experiments in the simulation, we set spike times during the CS to a constant 100-Hz frequency. To keep the strength of the CS input comparable with other probe protocols, we reduced the number of CS-driven mossy fibers in these experiments by half. An excitatory conductance was applied to the climbing fibers to represent the presentation of the US. Both types of simulations, with and without DCNcol, were trained for 2000 paired trials at a 500-ms ISI with a 5-s intertrial interval. In both types of simulations, the performance reached a plateau after 400 to 500 trials. After the training period, the plasticity was frozen so that synaptic weights would not change during subsequent CS-alone probe trials. We tested computer simulations with the same probe protocols as used in experiments. Probe trials were delivered with a 5-s intertrial interval. Each probe type was presented for over 200 trials with simultaneous recordings of simulation PC activity and eyelid behavioral data or for over 2000 trials if only eyelid behavioral data were collected. The simulated eyelid position was calculated as a smoothened sum of all DNC neuron action potentials with a decaying time constant that was passed through a threshold function. The amplitude of the simulated eyelid position was scaled such that the maximum CR amplitude over 2000 trials training period corresponded to a 6-mm eyelid closure. All simulations were run on a custom-built computer housing eight graphics cards (interfaced through CUDA, NVidia) totaling 12,286 GPU cores.

Analysis of simulation data was implemented in a way to parallel analysis of experimental data. For analysis of simulation PC activity, we randomly sampled different PCs over six trials of each probe type per cell to replicate session design used in experiments.

Histology

After the conclusion of experiments, the final placement of stimulation electrodes and tetrodes was determined by making small marking lesions. Each implanted electrode was marked by passing 100 μA of anodal dc for 10 s. A fraction of tetrodes (2 to 4 out of 16) was marked by passing 10 μA of anodal dc for 10 s. Animals were killed with an overdose of sodium pentobarbital and perfused intracardially with 0.9% saline (~1.0 liters), followed by 10% formalin (~1.0 liters). Heads were post-fixed in formalin for at least 3 days, after which stimulation electrodes and tetrodes were removed and the brains were extracted. Brains were then cryoprotected in 30% sucrose in formalin for 3 days, embedded in an albumin gelatin mixture, and the cerebellum was sectioned using a freezing microtome at 40 μm. Tissue was mounted on slides and stained with cresyl violet.

SUPPLEMENTARY MATERIALS

Supplementary material for this article is available at http://advances.sciencemag.org/cgi/content/full/4/5/eaap9660/DC1

Supplementary Materials and Methods

fig. S1. Distributions of CR amplitudes in response to different stimuli presentations.

fig. S2. CR probability as a function of probe.

fig. S3. CDF of CR amplitudes for subjects trained to produce half-sized CRs.

fig. S4. Isolation of single units and eyelid PCs from tetrode recordings.

fig. S5. Eyelid PC responses during sessions with short probes.

fig. S6. PC choice probabilities for individual probe types.

fig. S7. Acquisition of CRs in large-scale cerebellar simulations.

fig. S8. Definition of BI and relative PC response.

fig. S9. ROC analysis of PC activity from simulation with DCNcol.

table S1. Two-sample Kolmogorov-Smirnov test, comparison between CR amplitude distributions to probe and trained inputs.

table S2. Results of two-way ANOVA on PC spike counts to different probe inputs on CR and non-CR trials.

REFERENCES AND NOTES

1. D. J. Field, Relations between the statistics of natural images and the response properties of cortical cells. *J. Opt. Soc. Am. A* **4**, 2379–2394 (1987).
2. G. Tkačik, J. S. Prentice, V. Balasubramanian, E. Schneidman, Optimal population coding by noisy spiking neurons. *Proc. Natl. Acad. Sci. U.S.A.* **107**, 14419–14424 (2010).
3. J. Zylberberg, J. Cafaro, M. H. Turner, E. Shea-Brown, F. Rieke, Direction-selective circuits shape noise to ensure a precise population code. *Neuron* **89**, 369–383 (2016).
4. J. E. Dunsmoor, R. Paz, Fear generalization and anxiety: Behavioral and neural mechanisms. *Biol. Psychiatry* **78**, 336–343 (2015).
5. J. A. Tracy, G. B. Britton, J. E. Steinmetz, Comparison of single unit responses to tone, light, and compound conditioned stimuli during rabbit classical eyeblink conditioning. *Neurobiol. Learn. Mem.* **76**, 253–267 (2001).
6. T. Ohyama, W. L. Nores, M. D. Mauk, Stimulus generalization of conditioned eyelid responses produced without cerebellar cortex: Implications for plasticity in the cerebellar nuclei. *Learn. Mem.* **10**, 346–354 (2003).
7. M. Ito, The modifiable neuronal network of the cerebellum. *Jpn. J. Physiol.* **34**, 781–792 (1984).
8. D. Marr, A theory of cerebellar cortex. *J. Physiol.* **202**, 437–470 (1969).
9. J. F. Medina, W. L. Nores, T. Ohyama, M. D. Mauk, Mechanisms of cerebellar learning suggested by eyelid conditioning. *Curr. Opin. Neurobiol.* **10**, 717–724 (2000).
10. J. H. Freeman, Cerebellar learning mechanisms. *Brain Res.* **1621**, 260–269 (2015).
11. J. C. Kreider, M. D. Mauk, Eyelid conditioning to a target amplitude: Adding how much to whether and when. *J. Neurosci.* **30**, 14145–14152 (2010).
12. J. E. Steinmetz, D. G. Lavond, R. F. Thompson, Classical conditioning of the rabbit eyelid response with mossy fiber stimulation as the conditioned stimulus. *Bull. Psychon. Soc.* **23**, 245–248 (1985).
13. B. E. Kalmbach, H. Voicu, T. Ohyama, M. D. Mauk, A subtraction mechanism of temporal coding in cerebellar cortex. *J. Neurosci.* **31**, 2025–2034 (2011).
14. D. A. McCormick, R. F. Thompson, Cerebellum: Essential involvement in the classically conditioned eyelid response. *Science* **223**, 296–299 (1984).
15. P. Svensson, M. Ivarsson, Short-lasting conditioned stimulus applied to the middle cerebellar peduncle elicits delayed conditioned eye blink responses in the decerebrate ferret. *Eur. J. Neurosci.* **11**, 4333–4340 (1999).
16. D.-A. Jirenhed, G. Hesslow, Time course of classically conditioned Purkinje cell response is determined by initial part of conditioned stimulus. *J. Neurosci.* **31**, 9070–9074 (2011).
17. S. P. Perrett, M. D. Mauk, Extinction of conditioned eyelid responses requires the anterior lobe of cerebellar cortex. *J. Neurosci.* **15**, 2074–2080 (1995).
18. K. S. Garcia, P. M. Steele, M. D. Mauk, Cerebellar cortex lesions prevent acquisition of conditioned eyelid responses. *J. Neurosci.* **19**, 10940–10947 (1999).
19. H. E. Halverson, A. Khilkevich, M. D. Mauk, Relating cerebellar Purkinje cell activity to the timing and amplitude of conditioned eyelid responses. *J. Neurosci.* **35**, 7813–7832 (2015).
20. S. Ohmae, J. F. Medina, Climbing fibers encode a temporal-difference prediction error during cerebellar learning in mice. *Nat. Neurosci.* **18**, 1798–1803 (2015).
21. M. M. ten Brinke, H.-J. Boele, J. K. Spanke, J.-W. Potters, K. Kornysheva, P. Wulff, A. C. H. G. IJpelaar, S. K. E. Koekkoek, C. I. De Zeeuw, Evolving models of Pavlovian conditioning: Cerebellar cortical dynamics in awake behaving mice. *Cell Rep.* **13**, 1977–1988 (2015).
22. S. A. Heiney, J. Kim, G. J. Augustine, J. F. Medina, Precise control of movement kinematics by optogenetic inhibition of Purkinje cell activity. *J. Neurosci.* **34**, 2321–2330 (2014).
23. J. F. Medina, S. G. Lisberger, Encoding and decoding of learned smooth-pursuit eye movements in the floccular complex of the monkey cerebellum. *J. Neurophysiol.* **102**, 2039–2054 (2009).
24. D. J. Herzfeld, Y. Kojima, R. Soetedjo, R. Shadmehr, Encoding of action by the Purkinje cells of the cerebellum. *Nature* **526**, 439–442 (2015).
25. J. F. Medina, S. G. Lisberger, Links from complex spikes to local plasticity and motor learning in the cerebellum of awake-behaving monkeys. *Nat. Neurosci.* **11**, 1185–1192 (2008).
26. Y. Yang, S. G. Lisberger, Purkinje-cell plasticity and cerebellar motor learning are graded by complex-spike duration. *Nature* **510**, 529–532 (2014).
27. D. J. Herzfeld, Y. Kojima, R. Soetedjo, R. Shadmehr, Cerebellar complex spikes encode error direction and magnitude, *Society for Neuroscience Conference* (Society for Neuroscience, 2017); www.abstractsonline.com/pp8/#!/4376/presentation/7600.
28. K. H. Britten, W. T. Newsome, M. N. Shadlen, S. Celebrini, J. A. Movshon, A relationship between behavioral choice and the visual responses of neurons in macaque MT. *Vis. Neurosci.* **13**, 87–100 (1996).
29. S. Liu, Y. Gu, G. C. DeAngelis, D. E. Angelaki, Choice-related activity and correlated noise in subcortical vestibular neurons. *Nat. Neurosci.* **16**, 89–97 (2013).
30. J. D. T. Engbers, F. R. Fernandez, R. W. Turner, Bistability in Purkinje neurons: Ups and downs in cerebellar research. *Neural Netw.* **47**, 18–31 (2013).
31. J. F. Medina, M. D. Mauk, Computer simulation of cerebellar information processing. *Nat. Neurosci.* **3**, 1205–1211 (2000).
32. W.-K. Li, M. J. Hausknecht, P. Stone, M. D. Mauk, Using a million cell simulation of the cerebellum: Network scaling and task generality. *Neural Netw.* **47**, 95–102 (2013).
33. K.-F. Wong, X.-J. Wang, A recurrent network mechanism of time integration in perceptual decisions. *J. Neurosci.* **26**, 1314–1328 (2006).
34. B. D. Houck, A. L. Person, Cerebellar premotor output neurons collateralize to innervate the cerebellar cortex. *J. Comp. Neurol.* **523**, 2254–2271 (2015).
35. L. Ankri, Z. Husson, K. Pietrajtis, R. Proville, C. Léna, Y. Yarom, S. Dieudonné, M. Y. Uusisaari, A novel inhibitory nucleo-cortical circuit controls cerebellar Golgi cell activity. *eLife* **4**, e06262 (2015).
36. C. C. Guo, M. C. Ke, J. L. Raymond, Cerebellar encoding of multiple candidate error cues in the service of motor learning. *J. Neurosci.* **34**, 9880–9890 (2014).
37. J. F. Medina, S. G. Lisberger, Variation, signal, and noise in cerebellar sensory–motor processing for smooth-pursuit eye movements. *J. Neurosci.* **27**, 6832–6842 (2007).
38. P. Svensson, D.-A. Jirenhed, F. Bengtsson, G. Hesslow, Effect of conditioned stimulus parameters on timing of conditioned Purkinje cell responses. *J. Neurophysiol.* **103**, 1329–1336 (2010).
39. K. S. Garcia, M. D. Mauk, G. Weidemann, E. J. Kehoe, Covariation of alternative measures of responding in rabbit (*Oryctolagus cuniculus*) eyeblink conditioning during acquisition training and tone generalization. *Behav. Neurosci.* **117**, 292–303 (2003).
40. Z. Gao, M. Proietti-Onori, Z. Lin, M. M. ten Brinke, H.-J. Boele, J.-W. Potters, T. J. H. Ruigrok, F. E. Hoebeek, C. I. De Zeeuw, Excitatory cerebellar nucleocortical circuit provides internal amplification during associative conditioning. *Neuron* **89**, 645–657 (2016).
41. A. Giovannucci, A. Badura, B. Deverett, F. Najafi, T. D. Pereira, Z. Gao, I. Ozden, A. D. Kloth, E. Pnevmatikakis, L. Paninski, C. I. De Zeeuw, J. F. Medina, S. S.-H. Wang, Cerebellar granule cells acquire a widespread predictive feedback signal during motor learning. *Nat. Neurosci.* **20**, 727–734 (2017).
42. T. Ohyama, W. L. Nores, J. F. Medina, F. A. Riusech, M. D. Mauk, Learning-induced plasticity in deep cerebellar nucleus. *J. Neurosci.* **26**, 12656–12663 (2006).

43. T. D. B. Nguyen-Vu, R. R. Kimpo, J. M. Rinaldi, A. Kohli, H. Zeng, K. Deisseroth, J. L. Raymond, Cerebellar Purkinje cell activity drives motor learning. *Nat. Neurosci.* **16**, 1734–1736 (2013).
44. K. Lee, P. J. Mathews, A. M. B. Reeves, K. Y. Choe, S. A. Jami, R. E. Serrano, T. S. Otis, Circuit mechanisms underlying motor memory formation in the cerebellum. *Neuron* **86**, 529–540 (2015).
45. A. Khilkevich, H. E. Halverson, J. E. Canton-Josh, M. D. Mauk, Links between single-trial changes and learning rate in eyelid conditioning. *Cerebellum* **15**, 112–121 (2016).
46. G. Billings, E. Piasini, A. Lőrincz, Z. Nusser, R. A. Silver, Network structure within the cerebellar input layer enables lossless sparse encoding. *Neuron* **83**, 960–974 (2014).
47. R. C. O'Reilly, J. L. McClelland, Hippocampal conjunctive encoding, storage, and recall: Avoiding a trade-off. *Hippocampus* **4**, 661–682 (1994).
48. S. B. Ryan, K. L. Detweiler, K. H. Holland, M. A. Hord, V. Bracha, A long-range, wide field-of-view infrared eyeblink detector. *J. Neurosci. Methods* **152**, 74–82 (2006).
49. J. C. Eccles, Circuits in the cerebellar control of movement. *Proc. Natl. Acad. Sci. U.S.A.* **58**, 336–343 (1967).

Acknowledgments: We thank L. Nguyen, N. Keller, and B. Pandey for assistance with behavioral experiments; H. Halverson for assistance with tetrode recordings; M. Goldman and A. Kennedy for productive discussions regarding DCN feedback hypothesis; F. Riusech for assistance with histological work; and R. Chaudhuri and A. Huk for valuable comments on earlier versions of the manuscript. **Funding:** This work was supported by MH 46904 and NS98308 to M.D.M. **Author contributions:** A.K. and M.D.M. designed the study, A.K. and J.C.-J. performed the behavioral experiments, A.K. performed the in vivo recording experiments, E.D. implemented the experiments in cerebellar simulation, A.K. designed and performed all analyses, and A.K. and M.D.M. wrote the manuscript. **Competing interests:** The authors declare that they have no competing interests. **Data and materials availability:** All data needed to evaluate the conclusions in the paper are present in the paper and/or the Supplementary Materials. Additional data related to this paper may be requested from the authors.

Submitted 14 September 2017
Accepted 18 April 2018
Published 30 May 2018
10.1126/sciadv.aap9660

Citation: A. Khilkevich, J. Canton-Josh, E. DeLord, M. D. Mauk, A cerebellar adaptation to uncertain inputs. *Sci. Adv.* **4**, eaap9660 (2018).

Science Advances

A cerebellar adaptation to uncertain inputs

Andrei Khilkevich, Jose Canton-Josh, Evan DeLord and Michael D. Mauk

Sci Adv **4** (5), eaap9660.
DOI: 10.1126/sciadv.aap9660